Food Packaging and Shelf Life 31 (2022) 100797

Contents lists available at ScienceDirect

Food Packaging and Shelf Life

journal homepage: www.elsevier.com/locate/fpsl

A multiphysics approach for modeling gas exchange in microperforated films for modified atmosphere packaging of respiring products

Jaime González-Buesa [a,b,*], María L. Salvador [b]

[a] Unidad de Hortofruticultura, Centro de Investigación y Tecnología Agroalimentaria de Aragón (CITA), Instituto Agroalimentario de Aragón - IA2 (CITA-Universidad de Zaragoza), Av. Montañana 930, 50059 Zaragoza, Spain
[b] Grupo de Investigación en Alimentos de Origen Vegetal, Instituto Agroalimentario de Aragón-IA2-(Universidad de Zaragoza-CITA), Miguel Servet 177, 50013 Zaragoza, Spain

ARTICLE INFO

Keywords:
Modified atmosphere packaging
Microperforation
Fresh produce
Respiration
Mass transfer
Mathematical model

ABSTRACT

The objective of this work is to quantify, model and verify how the interactions between the respiring products and the surrounding atmosphere in a package affect the gas exchange through a microperforation. The pressure drop generated in a closed system by the metabolic activity of five different products has been determined by direct and indirect measurements. In this way, the estimated compensating hydrodynamic flows that can pass through the microperforated film ranged from 0.34 to 4.75 mL h^{-1}. A 3D model that considers the mass transfer coupled with the momentum transfer has been proposed to predict the gas concentration profiles around the microperforations originated by the diffusive and convective flows. A novel gas exchange measurement system, able to deliver small convective airflows comparable to those obtained for the different products and conditions, was assembled for the model verification. The model correctly predicts experimental data obtained for different convective flows.

1. Introduction

Modified atmosphere packaging (MAP) is a useful technology for reducing the quality loss and extending the shelf life of whole and fresh-cut fruits and vegetables. A perfect/ideal MAP would achieve the most appropriate gas composition for preserving each product, by means of the product's own respiration and the gas transfer through the packaging material. In general, low levels of O_2 and moderate levels of CO_2 may help to reduce product metabolism, microorganism growth, and weight loss. However, the low values of O_2 and CO_2 permeabilities of the polymeric materials do not allow the excess CO_2 to be removed or the addition of the necessary O_2 in order not to reach anaerobic conditions. The new biobased films used in MAP such as PLA do not seem to offer novelty in this respect (Curtzwiler, Vorst, Palmer & Brown, 2008; González-Buesa, Page, Kaminski, Ryser, Beaudry & Almenar, 2014; Mistriotis, Briassoulis, Giannoulis & D'Aquino, 2016; Peelman, Ragaert, De Meulenaer, Adons, Peeters & Cardon, 2013). Microperforated films are commonly used since their greater gas exchange assists MAP in adapting to the requirements of high respiration fresh food products such as minimally processed fruits and vegetables, and because they allow the CO_2/O_2 transfer ratio to be reduced due to the non-selective permeation through the perforation (Kartal, Aday, & Caner, 2012; Larsen & Liland, 2013). Thus, a wide range of atmospheres can be obtained combining the polymer matrix characteristics and the number and size of the perforations, normally with a diameter between 50 and 300 μm (Beaudry, 1999; Chung, Papadakis, & Yam, 2003; Techavises & Hikida, 2008; Xanthopoulos, Koronaki, & Boudouvis, 2012).

Most of the mathematical models proposed to simulate the gas exchange through a microperforated film consider that it can be described by the sum of two terms: diffusive flow through the film matrix and diffusive flow through the perforation (Belay, Caleb, & Opara, 2016). The latter contributes to the total flow to a greater extent (Sousa-Gallagher, Mahajan, & Mezdad, 2013; Zhang, Liu, & Geng, 2017), normally expressed by Fick's law (Castellanos, Cerisuelo, Hernandez-Muñoz, Herrera & Gavara, 2016; Chung, Papadakis, & Yam, 2003; Giannoulis, Mistriotis, & Briassoulis, 2017; Paul & Clarke, 2002) or the Maxwell-Stefan law (Renault, Souty, & Chambroy, 1994; Rennie & Tavoularis, 2009a).

The respiring product interactions with the surrounding atmosphere produces modifications in the gas composition and generates pressure

* Correspondence to: Unidad de Hortofruticultura, Centro de Investigación y Tecnología Agroalimentaria de Aragón (CITA), Av. Montañana 930, 50059 Zaragoza, Spain.
E-mail address: jgonzalez@cita-aragon.es (J. González-Buesa).

https://doi.org/10.1016/j.fpsl.2021.100797
Received 30 August 2021; Received in revised form 12 November 2021; Accepted 17 December 2021
Available online 30 December 2021

changes in the headspace of rigid or semi-rigid containers. A difference between the O_2 consumption rate and the CO_2 production rate is one of the main causes of these pressure changes. In fact, the respiratory quotient is usually between 0.7 and 1.3 (Kader, Zagory, & Kerbel, 1989), with higher oxygen consumption than CO_2 production being more common in most products (Hertog, Peppelenbos, Evelo & Tijskens, 1998). Other factors that can contribute to pressure drops are: the absorption of carbon dioxide and other species by the water contained in the product (Lee, 2016; Kusuma & Bugbee, 2020), moisture absorbers and gas scavengers (Lee, 2016; Jalali, Rux, Linke, Geyer, Pant & Saengerlaub, 2019), or differences in the permeation rates of the gases involved through the package. When these pressure drops occur in a package with microperforations, an air stream flows from the outside through the perforation to compensate for them. Some models have tried to consider this phenomenon by adding a convective term to the flow through the microperforation (Del-Valle, Almenar, Lagarón, Catalá & Gavara, 2003; González-Buesa, Ferrer-Mairal, Oria & Salvador, 2009). However, the entry of air from outside may generate a gas composition around the perforation different to that inside the package, and most of the proposed models do not contemplate the spatial dependence of the gas concentrations in the headspace. Consequently, the effect of the inward convective flow that attenuates the diffusive exit of CO_2 is undervalued. Some attempts have been made to take into account the fact that in the surroundings of the perforation the concentration of the different gases does not correspond to that in the rest of the package, adding an end correction term in the Fick equation to the length of the microperforation that depends on the hole diameter (Lee & Renault, 1998; Paul & Clarke, 2002; Abdellatief, Welt, Butler, McLamore, Teixeira & Shukla, 2015). However, these modifications have been shown to be insufficient in some cases (Castellanos *et al.* 2016; González-Buesa *et al.* 2009). One of the few space-time dependent models is that proposed by Rennie & Tavoularis (2009a), which considers four subdomains (the ambient atmosphere around the package, the perforation, the respiring commodity and the headspace inside the package), and includes convective and diffusive flow though the perforation. However, this model has been implemented for tubes, not for pinholes (Rennie & Tavoularis, 2009b). Another case is the 3D model developed by Giannoulis, Mistriotis, & Briassoulis (2017) for equilibrium modified atmosphere packaging using PLA films with perforations (0.2–8 mm in diameter). However, this does not consider the convective term in the transport of gases through the perforations.

The main objectives of this work were: (i) to verify, by direct measurements, the relevance of pressure drops generated by the interaction of different respiring products with the surrounding atmosphere in standard packaging conditions; (ii) to develop a mathematical model capable of adequately describing, in a non-stationary state, the gas exchange through a microperforation considering the spatial dependence of the gas composition and both the diffusive and convective flow through the perforation; (iii) to implement an experimental system where fluid dynamics conditions are similar to those generated inside microperforated packages of respiring products, replicating the pressure-driven flows generated by the product without the source of uncertainty which can be produced by the product itself; and (iv) to validate the diffusive-convective transfer model with the results obtained in the experimental system.

2. Material and methods

2.1. Determination of the pressure drop generated by respiring products

Since the objective was to determine the pressure drop due only to the product interactions with the surrounding atmosphere, the measurements were not carried out in a package in order to avoid the influence of the different gas permeation rates. A static respirometer as described in González-Buesa & Salvador (2019) was used with slight modifications. The device consisted of an airtight chamber (1250 mL) containing the product to be tested placed in a Peltier-cooled incubator (IPP 500, Memmert, Germany). The CO_2 and O_2 concentrations inside the respirometer chamber were recorded by a non-dispersive infrared CO_2 sensor (CO2 Engine BLG, Senseair AB, Delsbo, Sweden) and an optical O_2 sensor (Luminox LOX-02, SST Sensing Ltd., Coatbridge, UK). The pressure drop inside the chamber was determined monitoring the relative pressure with a bidirectional pressure sensor (AMS 5915–0100-D-B, Analog Microelectronics GmbH, Mainz, Germany), and rectifying the data with the pressure outside the respiration chamber, measured with an AMS 5915–1200-B sensor (Analog Microelectronics GmbH, Mainz, Germany). The experiments were conducted for five different products with varying respiration rates and respiratory quotients (apple, avocado, blueberry, broccoli florets, and strawberry) at two temperatures (4 and 23 °C). The weights of the products in the respirometer were: 459 ± 38 g for apple, 423 ± 5 g for avocado, 500 ± 1 g for blueberry, 204 ± 2 g for broccoli and 381 ± 3 g for strawberry. Three replicates for each product and temperature were performed, and data were recorded every 5 min

2.2. Experimental set-up

A custom-built system was assembled to measure the CO_2 transmission rate through microperforations in fluid dynamic conditions similar to those generated in the MAP of respiring products. In this way, it was intended to eliminate the deviations in the measurements that the presence of fruits or vegetables would undoubtedly originate, and to isolate the effect of the pressure gradient on both sides of the perforation from other disturbances. A schematic diagram of the experimental system is shown in Fig. 1.

The main element of the system was a gas exchange module that consists of two chambers. The lower one was a 1250 mL glass jar with a sealing cap (Familia Wiss Terrines, Le Parfait, Auvergne, France). In order to monitor the CO_2 concentration, a non-dispersive infra-red (NDIR) CO_2 sensor (k33 ICB 30%, Senseair AB, Sweden) was placed inside this part of the module. The upper chamber was an acrylic cylinder provided with a gas inlet with a diffuser and a gas outlet. The microperforation was placed between the two modules by drilling a 1 cm diameter hole in the middle section of the sealing cap and attaching the film containing the microperforation to the lid using epoxy glue. A customized press system gripping the two chambers was set to guarantee uniform and strong pressure on the lid, providing high levels of tightness in the system. The lower module was initially filled with atmospheric air while a continuous flow of 100 mL min^{-1} of a 21% CO_2 and 79% N_2 gas mixture was passed through the upper one using a mass flow controller (Brooks Instrument model 5850 TR, Hatfield, PA, USA). After this initial flush, a continuous flow of 30 mL min^{-1} was set.

In order to obtain pressure differences between the two chambers similar to those generated at both sides of the microperforation in the MAP of respiring products, an inlet air flow was delivered into the lower chamber. The air flow required to achieve this was of such a small magnitude (in the range of μL min^{-1}) that, to the best of our knowledge, there is no commercial equipment able to deliver it, so it was necessary to assemble it ad hoc. The proposed system delivered indirectly small air flows by using the gas displacement principle, integrating a pressure driven microfluidic system (Fluigent GmbH, Germany), two water reservoirs (A and B), and the appropriate hydraulic connections. An identical module with no air flow inlet was used as the control.

Atmospheric pressure was monitored using an absolute pressure sensor (AMS 5915–1200-B, Analog Microelectronics GmbH, Mainz, Germany). Furthermore, a pressure monitoring module, similar to the lower chamber of the gas exchange module, connected to a bidirectional differential pressure sensor (AMS 5915–020-D-B, Analog Microelectronics GmbH, Mainz, Germany) was set up in order to obtain better precision measuring of small atmospheric pressure fluctuations.

All the sensors were controlled using an Arduino UNO (Arduino SRL, Strambino, Italy), and the data obtained was stored every minute in a

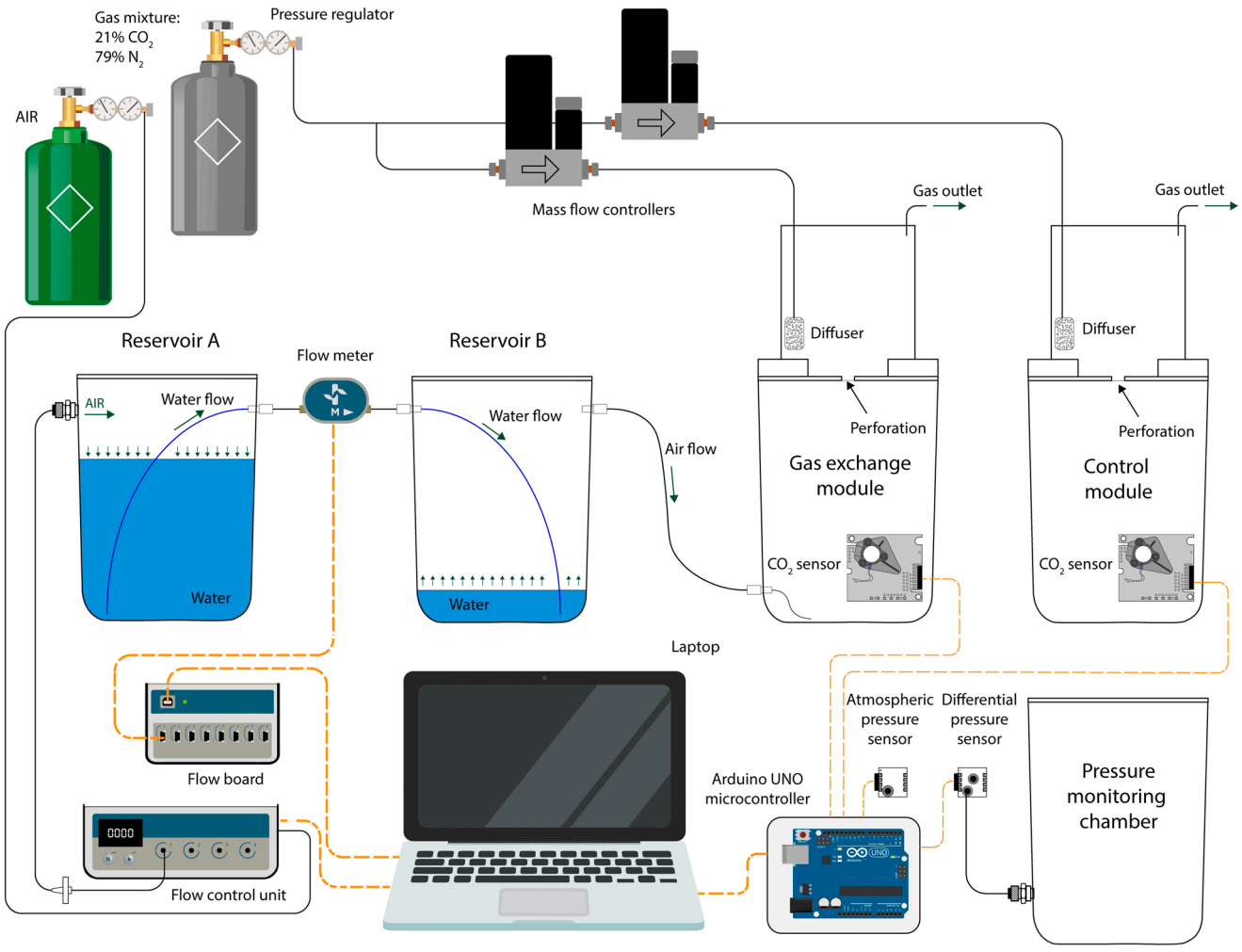

Fig. 1. Schematic diagram of the experimental set-up assembled to measure the CO_2 exchange through a microperforation when there are pressure differences between both sides of the microperforation similar to those generated in the MAP of respiring products.

laptop using the freeware software CoolTermWin (Roger Meier, CA, USA).

The CO_2 transmission rates through three microperforations were determined at 25 °C for air flows of 0, 0.6, 1.2, 2.4, and 4.8 mL h^{-1}. The dimensions of the three microperforations selected were, 125.7 ± 0.8 μm in length, 75.3 ± 0.6 μm in width, with a perimeter of 333.6 ± 3.0 μm, and an area of 7505.8 ± 40.0 μm^2. All experiments for each condition were conducted in triplicate, and data was recorded during approximately 300 h, if reservoir A was not completely depleted during the experiment.

2.3. Microperforations

The microperforations were chosen from 50 randomly selected previously from a 52.8 ± 1.3 μm-thick commercial microperforated film (AMCOR Flexibles, PPlus 52LD160, Ledbury, UK). These perforations were observed and pictured using a microscope at 20X (Axio Scope A1 AX10, Carl Zeiss Microscopy GmbH, Jena, Germany) with a 5 Megapixel camera (AxioCam Erc5s, Carl Zeiss Microscopy GmbH, Jena, Germany). The dimensions of the microperforations were obtained using the microscope software. The three microperforations selected were those with dimensions closest to the average values. The microperforations had a characteristic oval or ellipsoidal shape examined under the microscope. This shape has been found to depend on the stretching ratio of the film (Winotapun, Kerddonfag, Daud, Chinsirikul, Takarada & Kikutani, 2018) or the speed of the film during the perforation process (Varriano-Marston, 2006).

Different perforation cross sections were obtained using a cryo-ultramicrotome (EM UC7/FC7, Leica Microsystems GmbH, Wezlar, Germany). The samples were fixed on a cryo-ultramicrotome sample holder and trimmed at a temperature of − 110 °C, using a cryotrim 45 diamond knife (Diatome, Hatfield, PA, USA). The trimmed sample was then fixed on a specimen holder suitable for SEM observation, stuck with a double- sided carbon tape and coated with 14 nm of palladium. The perforations were visualized at 10 kV and spot size 3, using a field emission scanning electron microscope (Inspect F50, FEI Company, Hillsboro, OR, USA).

The cross-section and the view from different angles of a typical microperforation is shown in Fig. 2. Surface "a" has melted material accumulation around the perforation, while surface "b" is less damaged, as described as Winotapun, Aontee, Inyai, Pinsuwan, and Daud (2021) for a similar polyethylene terephthalate/polyethylene bilayer material. The pathway profile has the shape of a non-symmetrical double truncated cone. It is different from those described by other authors as a channel longer than the film thickness especially for PLA (Zhang, 2015), or as a circular rim which is formed surrounding the microhole (Winotapun et al., 2018).

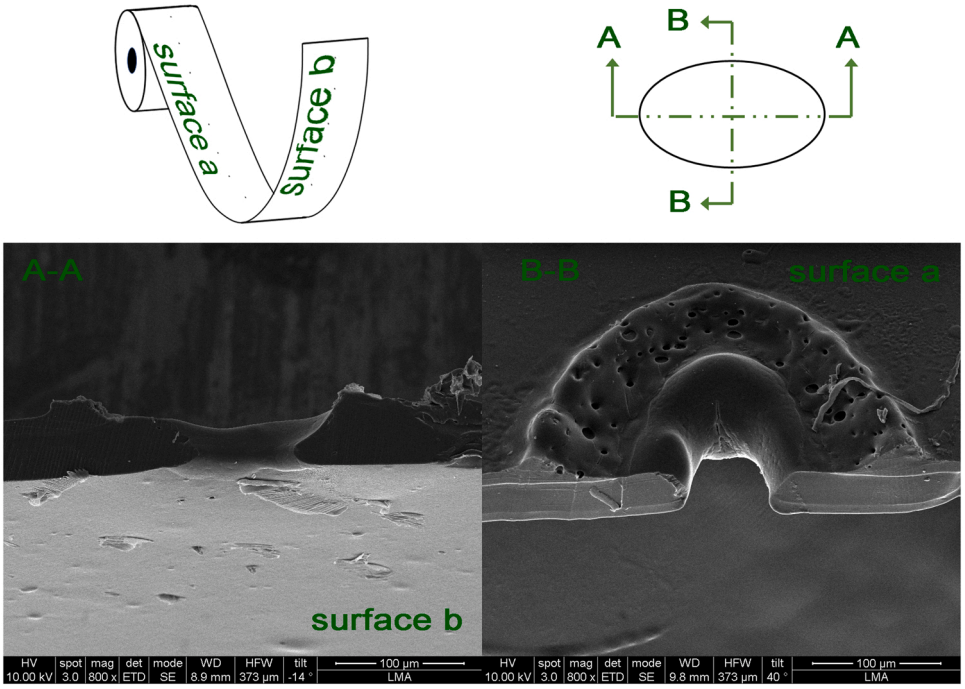

Fig. 2. SEM images of the microperforations. Cut through the major (A-A) and minor (B-B) axis.

2.4. Mathematical model

It is proposed that the gaseous exchange through a microperforation when there are differences in pressure and concentrations on both sides is a case of coupled transient mass and momentum transfer. The mass fraction ω_i of the different species (CO_2 or O_2) can be described using the Maxwell-Stefan diffusion and convection mass balance:

$$\rho\frac{\partial\omega_i}{\partial t}+\nabla\left(-\rho\omega_i\sum_{j=1}^{n}D_{ij}\left(\nabla x_j+\left(x_j-\omega_j\right)\frac{\nabla p}{p}\right)\right)=-\rho\boldsymbol{u}\nabla\omega_i \tag{1}$$

where t is the time, x_j is the mole fraction of species j, D_{ij} is the multicomponent Fick diffusivity matrix, p is the pressure, $\boldsymbol{u}$ is the velocity vector and ρ is the density calculated as:

$$\rho=\frac{p}{RT}\left(\sum\nolimits_i^n x_iM_i\right) \tag{2}$$

where M_i is the molecular weight of i species, R the gas constant and T the temperature. The binary gas diffusion coefficients for a gas pair ij, D_{ij}, are those recommended by Massman (1998), assuming the following dependence on pressure and temperature:

$$D_{ij}=D_{ij}(T_o,p_o)\left(\frac{p_o}{p}\right)\left(\frac{T}{T_o}\right)^{1.81} \tag{3}$$

The mass fraction of N_2 was calculated as the balance of the other mass fraction:

$$\omega_{N_2}=1-\omega_{O_2}-\omega_{CO_2} \tag{4}$$

Coupled to Eq. (1), the Navier-Stokes differential equations of compressible flow and the continuity equation were used to compute the velocity and pressure field inside the system. For constant temperature and for force volume and dilatational viscosity equal to zero, the equations are:

$$\rho\frac{\partial\boldsymbol{u}}{\partial t}+\rho(\boldsymbol{u}\nabla\boldsymbol{u})=\nabla\left(-p+\mu(\nabla\boldsymbol{u})-\left(\frac{2}{3}\mu(\nabla\boldsymbol{u})\boldsymbol{I}\right)\right) \tag{5}$$

$$\frac{\partial\rho}{\partial t}+\nabla(\rho\boldsymbol{u})=0 \tag{6}$$

where $\boldsymbol{I}$ is the identity matrix and μ is the dynamic viscosity, calculated as:

$$\mu=\sum\nolimits_{i=1}^{n}x_i\quad\mu_i \tag{7}$$

where $\mu_i$is the viscosity of the i specie.

A 3D computational model was developed to reproduce the gas exchange through a microperforation using COMSOL Multiphysics® v.3.5. This model included the two chambers of the gas exchange module of the experimental system described above (Fig. 1). Due to its rotational geometry, simulations were performed in a narrow section (corresponding to an angle of one degree) with symmetry boundary conditions on the side faces. The computational domain (Fig. 3) includes the top (Ω_1) and the bottom (Ω_2) chamber of the exchange module, the perforation channel (Ω_3), the CO_2-enriched gas entrance (Ω_4), and the air entrance (Ω_5). Full continuity was established between these subdomains. The external surfaces of the model matching with the outer limits of the gas exchange module were considered impermeable to gas exchange except for the bottom surface of the subdomain Ω_5, the upper surface of the subdomain Ω_4, and the side of the subdomain Ω_1. The lower surface of the subdomain Ω_5 was modeled as an inlet with constant CO_2 and O_2 molar fractions of 0.0005 and 0.2095, respectively, and an adjustable velocity depending on the flow delivered to the system. The upper surface of the subdomain Ω_4 was modeled as an inlet with constant velocity and CO_2 and O_2 molar fractions of 0.2095 and 0.0005, respectively. The side of the subdomain Ω_1 was set as an outlet with the pressure of the external environment. It was meshed with quad elements. The discretization consisted of 8550 elements and 8851 nodes. A finer mesh was formed close to the perforation and to the flow inlets. A mesh analysis showed no sensitivity of the results to mesh refinement. The direct Spooles solver was selected to solve the system of equations. The input parameters used in this model are shown in Table 1. These parameters were obtained through experimental test measurements or from the bibliography.

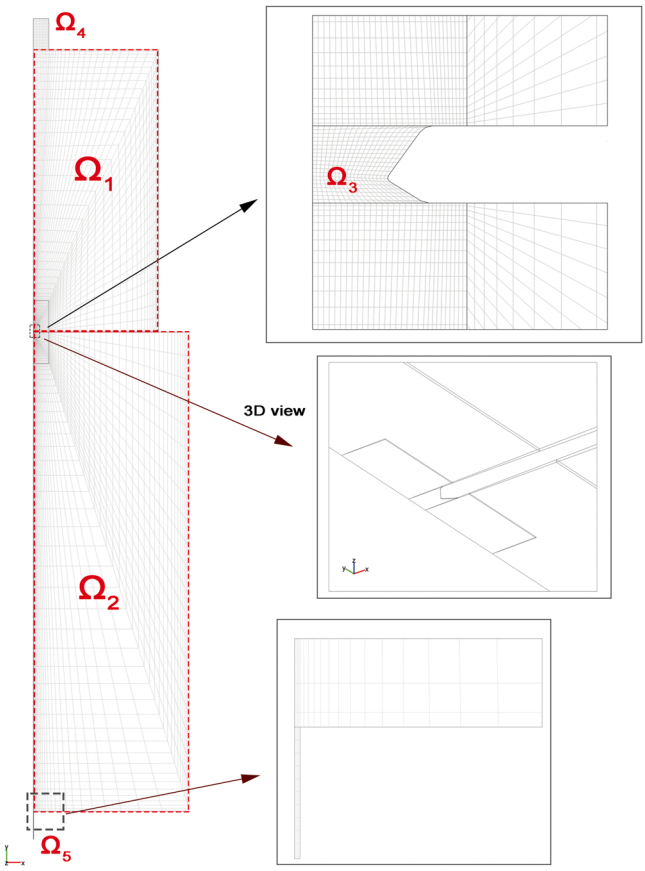

Fig. 3. Meshed computational domains.

Table 1
Model input parameters.

Name and description	Value	Source
T temperature [K]	298	measured
p initial atmospheric pressure [Pa]	99,104	measured
D_{O_2,N_2}(273 K, 101,325 Pa) [m^2 s^{-1}]	1.809e-5	Massman (1998)
D_{CO_2,O_2}(273 K, 101,325 Pa) [m^2 s^{-1}]	1.402e-5	Massman (1998)
D_{CO_2,N_2}(273 K, 101,325 Pa) [m^2 s^{-1}]	1.429e-5	Massman (1998)
R gas constant [J mol^{-1} K^{-1}]	8.314	–
μ_{O_2} O_2 viscosity [Pa·s]	2.050e-5	Comsol library
μ_{CO_2} CO_2 viscosity [Pa·s]	1.504e-5	Comsol library
μ_{N_2} N_2 viscosity [Pa·s]	1.770e-5	Comsol library
x_{O2_o} initial O_2 molar fraction	0.0005	measured
x_{CO2_o} initial CO_2 molar fraction	0.2095	measured
x_{N2_o} initial N_2 molar fraction	0.7900	measured

3. Results and discussion

3.1. Pressure drop generated by respiring products

For products in a microperforated package, the determination of the pressure drop created in a closed system by the metabolic activity of those products with different respiration rates was a necessary step in order to evaluate the driving pressure causing hydrodynamic flows through the microperforations.

The evolution over time of the differential pressure, P_{dif} (mbar), carbon dioxide concentration, [CO_2] (%) and oxygen concentration, [O_2], for the 5 selected products at 4 and 23 °C in the respirometer chamber is shown in Fig. 4. In all cases, the P_{dif} showed negatives values from the beginning or after a short period of time (<1 h), decreasing linearly with time. When critical O_2 and CO_2 levels were reached, an inflection point in the P_{dif} curve was detected, due to the presence of anaerobic metabolic routes, and thereafter the differential pressure began to increase due to the production of volatile compounds such as ethanol, acetaldehyde and other volatile compounds of the fermentative metabolism. This evolution is similar to that described by González-Buesa & Salvador (2019) for apple, cauliflower and strawberry. As expected, a decrease in the [O_2] and an increase in [CO_2] occurred at different rates that depend on the metabolism of each product. The temperature had a noticeable effect on P_{dif}, [O_2] and [CO_2], so that at 23 °C the products reached anoxic conditions after a few hours.

From the data available between 15% and 5% of [O_2], the respiration rates of O_2 and CO_2, R_{O2} and R_{CO2}, were determined. The RQ were calculated as constant values given the linear evolution of [O_2] and [CO_2] in this interval (Table 2). This [O_2] range is usual for steady [O_2] in the MAP of fresh and fresh-cut fruits and vegetables, including strawberries, blueberries or avocado (Almenar, Del-Valle, Hernández--Muñoz, Lagarón, Catalá & Gavara, 2007; Almenar, Samsudin, Auras, Harte & Rubino, 2008; Castellanos, Mendoza, Gavara & Herrera, 2017; Xanthopoulos, Koronaki, & Boudouvis, 2012). Thus, the calculated parameters in this range are appropriate for the actual product gas exchange during MAP storage. R_{O2} ranged from 1.88 ± 0.23 mL kg^{-1} h^{-1} for apple at 4 °C to 122.37 ± 12.34 mL kg^{-1} h^{-1} for broccoli florets at 23 °C, showing a great variability in the selected products. In all cases, R_{CO2} was lower than R_{O2} ranging from 1.14 ± 0.50 mL kg^{-1} h^{-1} for apple at 4 °C to 103.84 ± 10.87 mL kg^{-1} h^{-1} for broccoli florets at 23 °C. Thus, the RQ for the five different products and conditions was below 1, and the negative values observed for P_{dif} support this fact. The values of the RQ obtained, especially at low temperatures, were in some cases lower than those reported by other authors for these products (Beaudry, Cameron, Shirazi & Dostal-Lange, 1992; Exama, Arul, Lencki, Lee & Toupin, 1993; Ho, Verboven, Verlinden, Schenk, Delele & Rolletschek, 2010). This could be due to the different methodologies and conditions used for the determinations. However, for avocado Hertog, Nicholson, & Whitmore (2003) obtained at 7 °C a RQ of 0.5, a value very close to that obtained in this study. The high solubility of CO_2 in water (approximately 1.5 and 0.8 mL CO_2 STP/mL water at 4 and 23 °C, respectively) is another factor that can affect the results. The absorption of this gas in the tissues of the product undoubtedly favors the underestimation of the RQ, and partly explains the influence of the temperature on this parameter (Waghmare, Mahajan & Annapure, 2013). In fact, Bessemans et al. (2021) and Renault, Houal, Jacquemin, and Chambroy (1994) attributed to the absorption of CO_2 the low RQ obtained for pears at 0 °C (0.65) and strawberries at 10 °C (0.62–0.72), respectively. These last values are consistent with those shown in the present study.

The conditions that can lead to underestimated RQ values are the same as those which these products will have in MAP (changing gaseous composition inside the package, reduced levels of O_2, accumulation of CO_2, absorption of CO_2 in the tissues…). Therefore, the pressure drop that has been quantified would be the same in MAP with microperforated film if not compensated for by a hydrodynamic flow through the microperforations. The required flow to balance out the pressure drop in the respiration chamber was calculated from the pressure drop rate in two ways: from P_{dif} data (direct), and from the differences between R_{O2} and R_{CO2} (indirect), (Table 2). In the direct method, the flow was calculated from the slope of linear evolution of P_{dif} with time. To transform this rate of pressure drop into flow, it was necessary to know the free volume of the respiration chamber (for which it was considered the density of the products equal to 1 kg L^{-1}) and apply the ideal gas equation. In the indirect method, the flow rate was calculated by multiplying the weight of the product by the difference between R_{O2} and R_{CO2}. Regardless of the calculation method, the temperature and the product, the flow rates thus obtained from experimental data are between 0.27 and 4.75 mL h^{-1} (Table 2). These values indicate the air flows that was reasonable to introduce into reservoir B of the

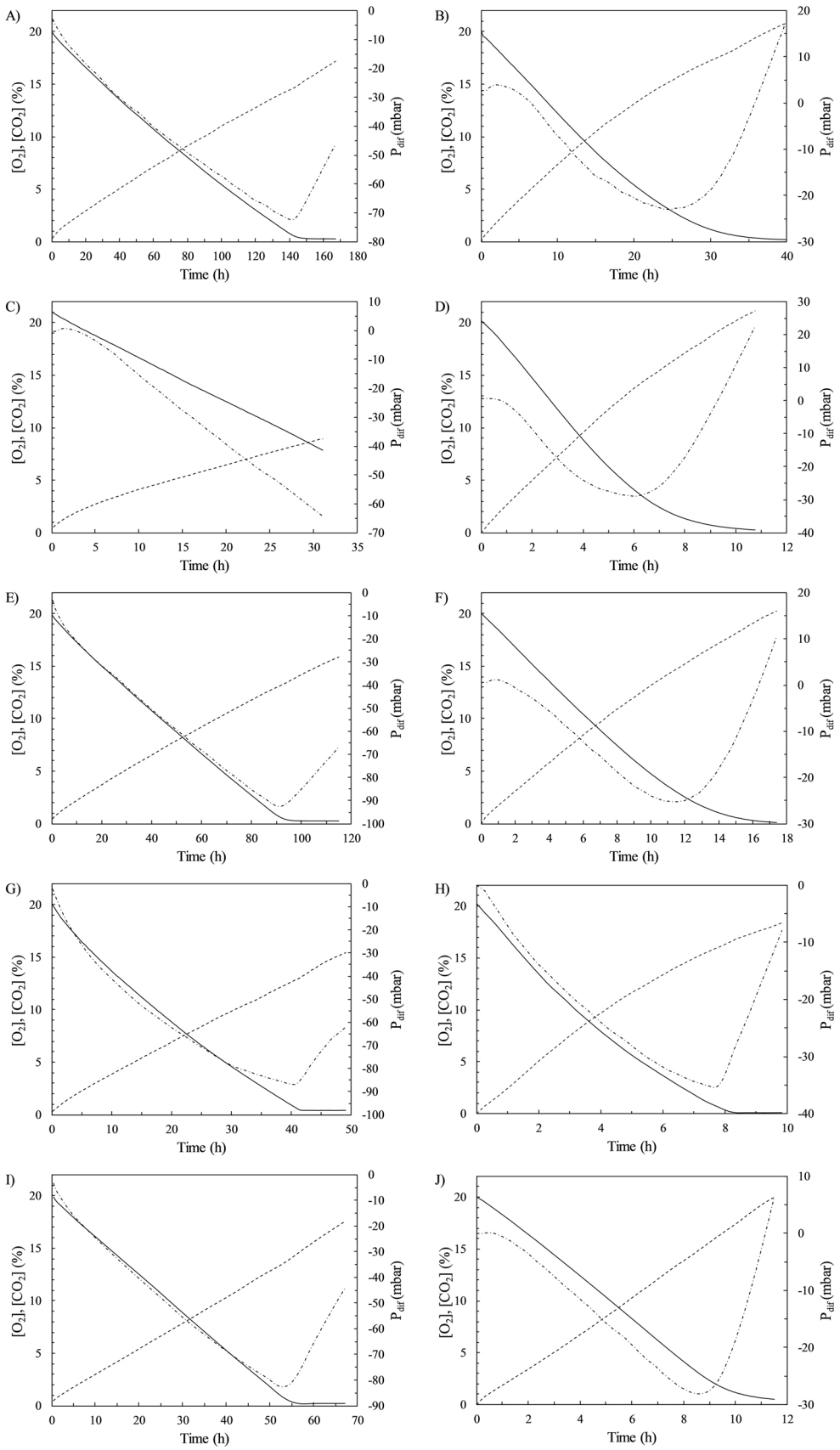

Fig. 4. Evolution of the O_2 concentration ([O_2], solid line), CO_2 concentration ([CO_2], dashed line), and differential pressure, (P_{dif}, dashed-dot line) in the closed-system respirometer at 4 °C for apple (A), avocado (C), blueberry (E), broccoli (G) and strawberry (I) and at 23 °C for apple (B), avocado (D), blueberry (F), broccoli (H) and strawberry (J).

Table 2
Respiration rates (R_{O2} and R_{CO2}), respiratory quotients (RQ), pressure drop rates and compensatory flows for the different products.

T [°C]	Product	R_{O2}[mL kg^{-1} h^{-1}]	R_{CO2}[mL kg^{-1} h^{-1}]	RQ	Indirect pressure drop rate[mbar h^{-1}]	Indirect flow [mL h^{-1}]	Direct pressure drop rate[mbar h^{-1}]	Direct flow[mL h^{-1}]
4	Apple	1.88 ± 0.23	1.14 ± 0.5	0.71 ± 0.02	0.36 ± 0.01	0.27 ± 0.01	0.46 ± 0.01	0.34 ± 0.00
	Avocado	8.88 ± 1.41	4.88 ± 0.98	0.55 ± 0.03	2.07 ± 0.23	1.69 ± 0.19	2.52 ± 0.27	2.06 ± 0.22
	Blueberry	3.31 ± 0.27	2.09 ± 0.07	0.63 ± 0.03	0.82 ± 0.13	0.61 ± 0.1	1.00 ± 0.13	0.74 ± 0.09
	Broccoli	24.61 ± 315	16.31 ± 1.55	0.66 ± 0.03	1.64 ± 0.36	1.69 ± 0.37	1.95 ± 0.23	2.01 ± 0.24
	Strawberry	8.58 ± 0.29	5.91 ± 0.29	0.69 ± 0.01	1.18 ± 0.02	1.01 ± 0.01	1.51 ± 0.06	1.29 ± 0.05
23	Apple	11.33 ± 2.65	9.52 ± 2,37	0.84 ± 0.02	0.97 ± 0.14	0.78 ± 0.12	1.21 ± 0.31	0.98 ± 0.26
	Avocado	57.75 ± 4.63	48.08 ± 0.98	0.83 ± 0.04	5.00 ± 0.69	4.08 ± 0.56	5.82 ± 0.08	4.75 ± 0.07
	Blueberry	23.26 ± 0.85	19.25 ± 0.56	0.83 ± 0.01	2.71 ± 0.22	2.00 ± 0.16	3.4 ± 0.28	2.52 ± 0.21
	Broccoli	122.37 ± 12.34	103.84 ± 10.87	0.85 ± 0.01	3.67 ± 0.43	3.79 ± 0.44	4.6 ± 0.21	4.74 ± 0.22
	Strawberry	46.98 ± 0.96	41.45 ± 1.79	0.88 ± 0.02	2.47 ± 0.44	2.12 ± 0.36	3.66 ± 0.34	3.13 ± 0.28

experimental system (Fig. 1) to simulate the MAP of a respiring product with a RQ < 1.

For the same product and conditions, the direct flows gave higher values than indirect flows. This imbalance between the two procedures may be due to a combination of several factors, although possibly the main factor is the absorption of the CO_2 in the product tissues. The implications of the absorption of CO_2 in the tissues for respiration rate measurements has been previously described by Saltveit (2012).

The measurement of the pressure drop rate from P_{dif} data provides a direct and more precise flow computation, if compared with estimated flows calculated through respiration differences, since it sums different factors and variables, providing a more reliable flow estimation. These values, ranging from 0.34 ± 0.01 mL h^{-1} for apple at 4 °C to 4.75 ± 0.07 mL h^{-1} for avocado at 23 °C, allow us to replicate in our experimental system the real hydrodynamic flows that pass through a microperforation of a package to compensate for the pressure drop caused by the respiration of the products, and to evaluate how this flow affects the composition of the atmosphere in the vicinity of the microperforation and therefore the diffusive transport.

As an example, to facilitate understanding of the magnitude of the phenomenon, and assuming a typical microperforation (7500 μm^2), the pressure-driven flow produced by 500 g of apple at 4 °C in a 1250 mL package will result in a velocity of 1.53 cm s^{-1} in the perforation, while it would be 20.73 cm s^{-1} for 200 g of broccoli florets at 23 °C. Furthermore, considering a constant entry of fresh air during 24 h of storage of these products, this would be 1.7 mL or 24 mL of oxygen entering the package, respectively. Depending on the free volume of the package, this entry of fresh air during storage could certainly be significant and has the potential of altering the headspace composition.

3.2. Measurement and modeling of the gas exchange through a microperforation

Using the experimental system designed for this purpose (Fig. 1), tests were carried out by introducing different air flows, f, into the lower chamber of the gas exchange module, within the range of pressure-driven flows produced by the product respiration and that have been experimentally determined (from f=0 to f=4.8 mL h^{-1}). The [CO_2] evolution over time in the lower chamber due to the gas exchange through the perforation is shown in Fig. 5 for the different air flows. The results obtained in the control module have also been included. As expected, the larger the air flow introduced into the gas exchange module, the smaller the amount of [CO_2] accumulation in the system. The fresh air entering the system mixes with the CO_2 enriched air in the chamber, increasing the pressure in the bottom chamber, and the gas mixture flows to the top chamber through the perforation to maintain equal pressure in both chambers.

Some models consider the additive approach according to which the transmission of gases through the microperforation involves both convection (flow required to compensate for the pressure) and diffusion (owing to partial pressure gradients) (Del-Valle *et al.* 2003; González-Buesa *et al.* 2009; Paul & Clarke, 2002; Ratti, Rabie, & Raghavan, 1998). These models should be able to model the gas composition evolution, even when hydrodynamic flows are present. However, the application of a previous model (González-Buesa *et al.* 2009), which includes the hydrodynamic flows created by pressure gradients due to imbalances in the diffusion coefficients plus the bulk flow as a result of the gap between R_{O2} and R_{CO2}, failed to simulate the [CO_2] evolution while the air flow was increased (Fig. 5, dashed line). The transmission rate used in these simulations was that obtained from the [CO_2] evolution data in the control chamber, 115.42 ± 5.33 mL CO_2 d^{-1}. The proposed model contemplates a rigorous treatment of the gas as a ternary mixture. Nevertheless, the previous models considered the gas phase as a binary (Ratti, Rabie, & Raghavan, 1998) or as a pseudo-binary mixture, so that the diffusive coefficient of component *i* in the mixture was estimated from the binary values (Del-Valle *et al.* 2003); or they considered the binary diffusion coefficients to be so similar that any selectivity of diffusive transport through the perforation was ignored (Paul & Clarke, 2002). Furthermore, these models applied Poiseuille's law to describe the hydrodynamic flow caused by a pressure gradient (Del-Valle *et al.* 2003; González-Buesa *et al.* 2009) but, unlike the proposed model, they did not consider the concentration gradient generated around the perforation as a consequence of the velocity field.

The newly developed multiphysics model, coupling Maxwell-Stephan equations for mass transfer and compressible Navier-Stokes equations for momentum transfer, was able to predict accurately the evolution of the [CO_2] in the control module, and the [CO_2] evolution for the different air flows introduced into the gas exchange module (Fig. 5, solid lines). The Root Mean Squared Errors, RMSE, for the [CO_2] for each case were: 0.083% for control, 0.181% for f= 0 mL h^{-1}, 0.232% for f= 0.6 mL h^{-1}, 0.113% for f= 1.2 mL h^{-1}, 0.182% for f= 2.4 mL h^{-1} and 0.160% for f= 4.8 mL h^{-1}.

To illustrate how the different convective flows affect the velocity field, the [CO_2] around the microperforation and therefore the diffusive transfer through the microperforation, the model solution are represented qualitatively and quantitatively in Figs. 6 and 7, respectively. Since the pictures represent the simulation after one-hour duration, the [CO_2] in the bottom chamber will be almost the same for the five different scenarios, enabling the comparison. As shown in the figure, the velocity at the center of the microperforation increases up to 30 cm s^{-1} for the maximum air flow. These flows, especially the higher ones, are strong enough to create a different [CO_2] profile around the perforation, particularly at the microperforation channel. The influence of these flows is shown in Fig. 7. In the lower chamber, the same CO_2 concentration line is flatter and closer to the microperforation as the flow increases, while in the upper chamber, the opposite occurs. This is quite remarkable, since the conditions around the microperforations determine the gas exchange. The fact that gas concentrations at the perforation surroundings may not be equal to the concentration in the bulk gas is taken into account in some models based on Fick's law of diffusion, adding a correction term to the diffusion path length, L. The evaluation of the end correction term is problematic, as indicated by the

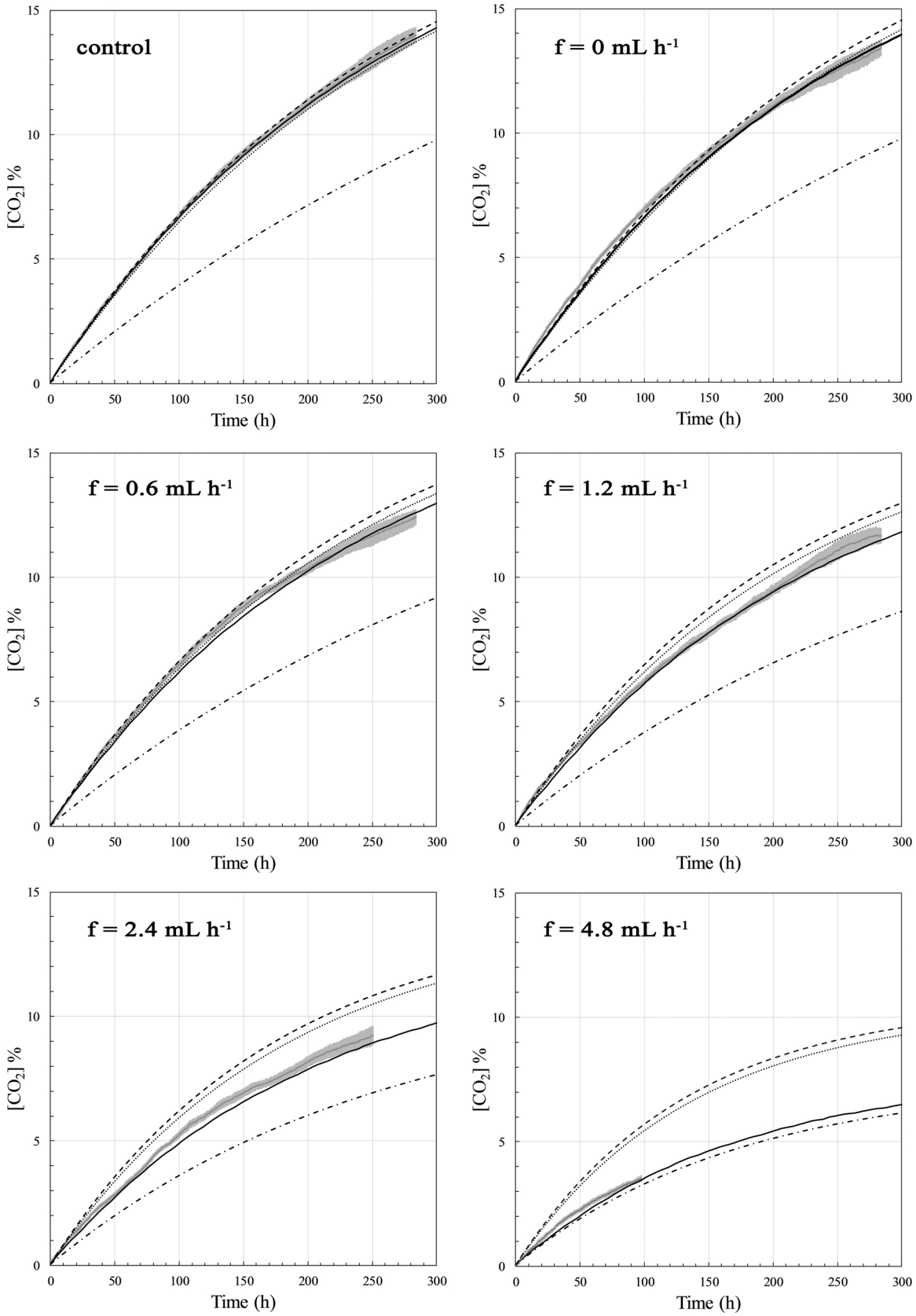

Fig. 5. Evolution of CO_2 concentration, $[CO_2]$, in the lower chamber of the control module and of the gas exchange module for different convective flows: experimental data (gray line), standard deviation of the experimental data (gray band), model prediction (solid line), previous model prediction (González et al., 2009, dashed line), previous model with a corrector term in the path length (L+0.4d, dot line, and L+1.1d, dashed-dot line).

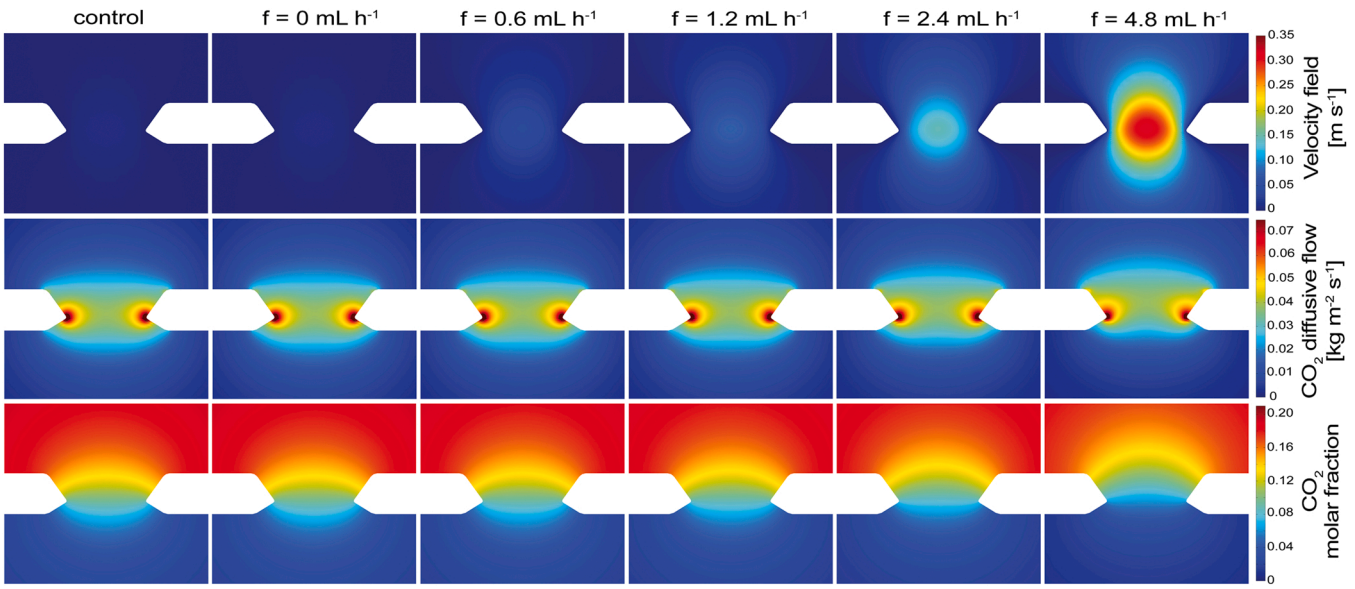

Fig. 6. Model solution after 1 h of simulation: velocity field, CO_2 diffusive flow and CO_2 molar fraction distribution around the perforation for control conditions and for different convective flows.

different assigned values (between 0.4 and 1.1 times the diameter of the perforation, d) (Fishman, Rodov, & Ben-Yehoshua, 1996; Chung, Papadakis, & Yam, 2003; Giannoulis, Mistriotis, & Briassoulis, 2017; Lange, Büsing, Hertlein & Hediger, 2000; Paul & Clarke, 2002; Lee & Renault, 1998; Ghosh & Anantheswaran, 2001, Mistriotis *et al.* 2016). In order to verify the effect of this corrector term, the previous model of González-Buesa *et al.* (2009) has been solved applying the transmission rates that correspond to a path length of L+ 0.4 d and L+ 1.1 d (108 mL CO_2 d^{-1} and 61.5 mL CO_2 d^{-1}, respectively). Surprisingly, the evolution of the [CO_2] for a path length of L+ 0.4d matches the experimental data for the control, while the evolution of the [CO_2] for a path length of L+ 1.1d matches the experimental data for f= 4.8 mL h^{-1}. Thus, the intermediate scenarios may be covered by adjusting the correction term. The model proposed in this work eliminates the arbitrariness of other models when assigning the path length value, and is capable of fitting to the experimental data under several conditions by considering the spatial variation of the [CO_2].

The gas concentration gradients around the microperforation could explain the mismatches found between the experimental data and the model predictions by Castellanos *et al.* (2016) and González-Buesa *et al.* (2009). The gas exchange through the microperforation was lower than predicted by the model. Both models have in common the fact that packages with very few microperforations were used for the experimental validations, thus the effects of the pressure-driven flows may play an important role in the microperforation gas exchange.

There are very few models to describe gas exchange through microperforations considering the spatial dependence of the gas concentrations. The 3D model proposed by Giannoulis, Mistriotis, & Briassoulis (2017) is one of them. However, it is simplified to a single diffusion transfer, considering as negligible the mass transport due to pressure-driven flow (RQ=1). They obtained good fitting results for packaged tomato and peach, using a moderate number (5) of big microperforations (200 μm diameter) per package. In that case, even if a pressure drop had occurred inside the package, the velocity of the compensation air coming into each microperforation would have had a small magnitude, not affecting the final result. Pressure-driven flows may be masked in packages with a high number of microperforations or perforations with large dimensions. This would explain the ability of several simplified models to fit the gas composition evolution in MAP taking into consideration the gas exchange through microperforations and the respiration rates of the products (Renault et al., 1994; Fishman, Rodov, & Ben-Yehoshua, 1996; Kwon, Jo, An, and Lee (2013); Sousa-Gallagher & Mahajan, 2013; Giannoulis, Mistriotis, & Briassoulis, 2017).

4. Conclusions

The experimental measurement of pressure drops in a closed system for five products of different metabolic activity and two temperatures provides valuable information about the product interaction with the surrounding atmosphere under different scenarios, together with a direct measurement of what would occur in a package, at least for the first days of storage. In a microperforated package, this pressure drop will generate a compensating pressure-driven flow through the microperforation. This pressure-driven flow has been recreated in the experimental system, isolating this factor from other disturbances that could alter it. The pressure-driven flow is big enough to generate concentration profiles around the microperforation that differ from those existing when there is no such flow, causing a decrease in the CO_2 diffusive flow in the bottom chamber of the gas exchange measurement module. These facts, which were postulated as mere hypotheses to explain that some models were not capable of predicting the evolution of the gas composition inside packages with few microperforations of reduced size, have been evidenced in this work.

The proposed 3D coupled mass and momentum transfer computational model, based on Maxwell-Stefan and Navier-Stokes equations, has adequately predicted the gas exchange through a microperforation for a wide range of pressure-driven flows (from 0 to 4.8 mL h^{-1}). Although this model has been implemented in a rigid system, it could be applied to a semi-rigid package since the inclusion of a very tiny hole will allow a convective flow to balance the pressure inside and outside the package.

Experimental determinations of the gas transmission rates in microperforations reported by various authors are in general aligned, and several MAP models have been proposed based on Fick's laws. According to the data obtained, these simplified models would be valid when the pressure-driven flow through each microperforation is small (< 1 mL h^{-1}), but tend to fail in other conditions.

Presumably the application of the Maxwell-Stefan equations is an unjustified complication since the various binary diffusion coefficients are so similar (Chung, Papadakis, & Yam, 2003; Paul & Clarke, 2002), thus the application of a simplified multiphysics computational model could be developed simply assuming Fick's law of diffusion for mass

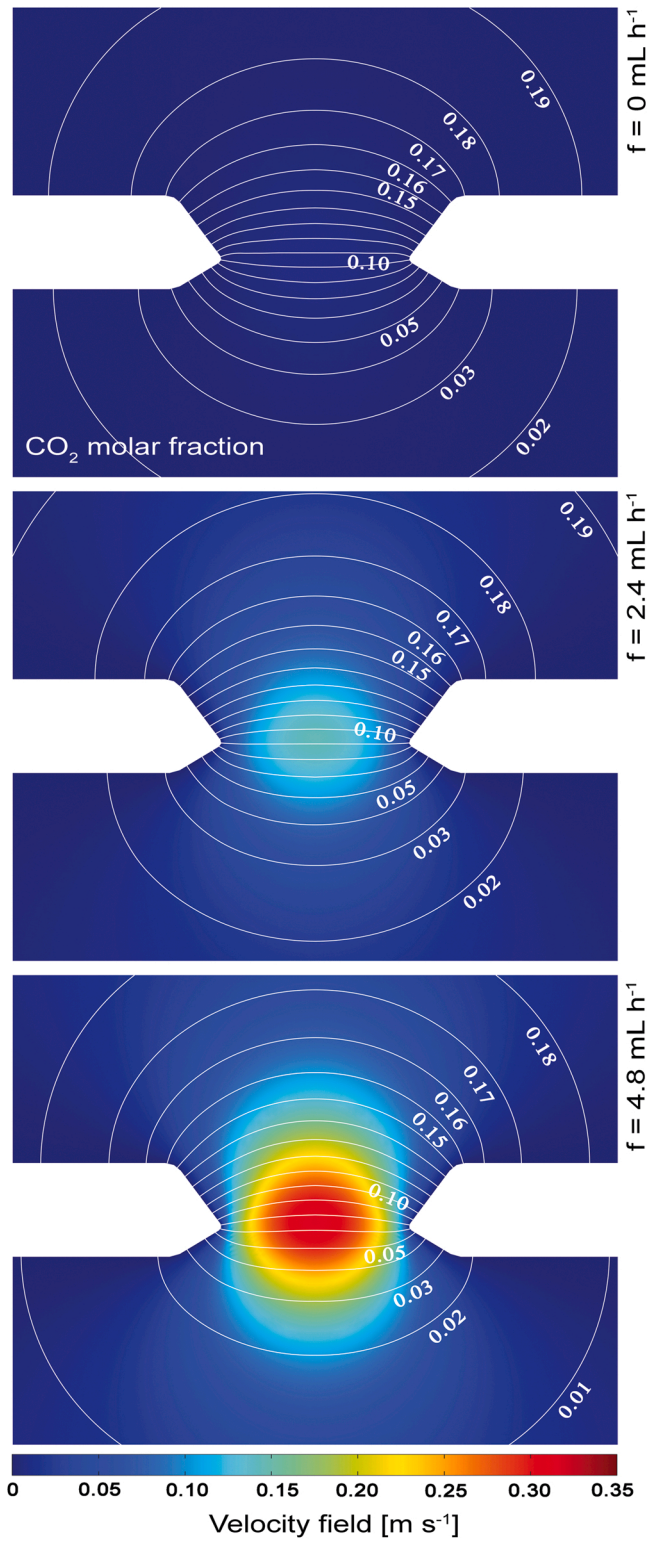

Fig. 7. Model solution after 1 h of simulation: CO_2 concentration lines around the perforation for different convective flows (0, 2.4 and 4.8 mL h^{-1}).

transfer. This may reduce the model complexity and probably reduce computing time, but the model performance should be checked. The next steps would be the improvement of the model taking into account the water vapor and therefore the transpiration of the product, and the implementation of the model in real MAP using microperforated films and different fruits and vegetables.

CRediT authorship contribution statement

Jaime González-Buesa: Conceptualization, Methodology, Investigation, Validation, Software, Visualization, Writing – original draft, Writing – review & editing, Funding acquisition. **María L. Salvador:** Conceptualization, Methodology, Resources, Writing – original draft, Writing – review & editing, Supervision.

Declaration of Competing Interest

The authors have no competing interests to declare.

Acknowledgments

This work was supported by the Instituto Nacional de Investigación y Tecnología Agraria y Alimentaria of Spain (INIA-DOC fellowship to J. González-Buesa), the Ministerio de Ciencia e Innovación of Spain (PID2019–108080RR-100), and the Seventh Framework Programme of the European Union (FP7/2007–2013) under REA grant agreement n° 332201. The SEM images were generated at the "Laboratorio de Microscopias Avanzadas" at the Universidad de Zaragoza. The authors acknowledge the LMA for offering access to their instruments and expertise.

References

Abdellatief, A., Welt, B. A., Butler, J., McLamore, E., Teixeira, A., & Shukla, S. (2015). Predictive modeling of oxygen transmission through micro-perforations for packaging applications. *Journal of Applied Packaging Research, 7*, 17–31. https://doi.org/10.14448/japr.04.0001

Almenar, E., Del-Valle, V., Hernández-Muñoz, P., Lagarón, J. M., Catalá, R., & Gavara, R. (2007). Equilibrium modified atmosphere packaging of wild strawberries. *Journal of the Science of Food and Agriculture, 87*, 1931–1939. https://doi.org/10.1002/jsfa.2938

Almenar, E., Samsudin, H., Auras, R., Harte, B., & Rubino, M. (2008). Postharvest shelf life extension of blueberries using a biodegradable package. *Food Chemistry, 110*, 120–127. https://doi.org/10.1016/j.foodchem.2008.01.066

Beaudry, R. M. (1999). Effect of O_2 and CO_2 partial pressure on selected phenomena affecting fruit and vegetable quality. *Postharvest Biology and Technology, 15*, 293–303. https://doi.org/10.1016/S0925-5214(98)00092-1

Beaudry, R. M., Cameron, A. C., Shirazi, A., & Dostal-Lange, D. L. (1992). Modified-atmosphere packaging of blueberry fruit: effect of temperature on package O_2 and CO_2. *Journal of the American Society for Horticultural Science, 117*, 436–441. https://doi.org/10.21273/JASHS.117.3.436

Belay, Z. A., Caleb, O. J., & Opara, U. L. (2016). Modelling approaches for designing and evaluating the performance of modified atmosphere packaging (MAP) systems for fresh produce: A review. *Food Packaging and Shelf Life, 10*, 1–15. https://doi.org/10.1016/j.fpsl.2016.08.001

Bessemans, N., Verlinden, B. E., Janssens, M., Verboven, P., Hertog, M. L. A. T. M., & Nicolaï, B. M. (2021). A modelling approach to explain low apparent RQ-measurements of (D)CA stored Conference pear fruit. *Acta Horticulturae, 1311*, 249–256. https://doi.org/10.17660/ActaHortic.2021.1311.31

Castellanos, D. A., Cerisuelo, J. P., Hernandez-Muñoz, P., Herrera, A. O., & Gavara, R. (2016). Modelling the evolution of O_2 and CO_2 concentrations in MAP of a fresh product: Application to tomato. *Journal of Food Engineering, 168*, 84–95. https://doi.org/10.1016/j.jfoodeng.2015.07.019

Castellanos, D. A., Mendoza, R., Gavara, R., & Herrera, A. O. (2017). Respiration and ethylene generation modeling of "Hass" avocado and feijoa fruits and application inmodified atmosphere packaging. *International Journal of Food Properties, 20*, 333–349. https://doi.org/10.1080/10942912.2016.1160921

Chung, D., Papadakis, S. E., & Yam, K. L. (2003). Simple models for evaluating effects of smalls leaks on the gas barrier properties of food packages. *Packaging Technology and Science, 16*, 77–86. https://doi.org/10.1002/pts.616

Curtzwiler, G., Vorst, K., Palmer, S., & Brown, J. W. (2008). Characterization of current environmentally-friendly films. *Journal of Plastic Film and Sheeting, 24*, 213–226. https://doi.org/10.1177/8756087908100836

Del-Valle, V., Almenar, E., Lagarón, J. M., Catalá, R., & Gavara, R. (2003). Modelling permeation through porous polymeric films for modified atmosphere packaging. *Food Additives and Contaminants, 20*, 170–179. https://doi.org/10.1080/0265203021000042869

Exama, A., Arul, J., Lencki, R. W., Lee, L. Z., & Toupin, C. (1993). Suitability of plastic films for modified atmosphere packaging of fruits and vegetables. *Journal of Food Science, 58*, 1365–1370. https://doi.org/10.1111/j.1365-2621.1993.tb06184.x

Fishman, S., Rodov, V., & Ben-Yehoshua, S. (1996). Mathematical model for perforation effect on oxygen and water vapor dynamics in modified atmosphere packages. *Journal of Food Science, 61*, 956–961. https://doi.org/10.1111/j.1365-2621.1996.tb10910.x

Giannoulis, A., Mistriotis, A., & Briassoulis, D. (2017). 3D numerical simulations as optimization tool for the design of novel EMAP systems. *Computers and Electronics in Agriculture, 143*, 119–129. https://doi.org/10.1016/j.compag.2017.10.004

Ghosh, V., & Anantheswaran, R. C. (2001). Oxygen transmition rate through micro-perforated films: measurement and model comparison. *Journal of Food Process Engineering, 24*, 113–133. https://doi.org/10.1111/j.1745-4530.2001.tb00535.x

González-Buesa, J., Ferrer-Mairal, A., Oria, R., & Salvador, M. L. (2009). A mathematical model for packaging with microperforated films of fresh-cut fruits and vegetables. *Journal of Food Engineering, 95*, 158–165. https://doi.org/10.1016/j.jfoodeng.2009.04.025

González-Buesa, J., Page, N., Kaminski, C., Ryser, E. T., Beaudry, R., & Almenar, E. (2014). Effect of non-conventional atmospheres and bio-based packaging on the quality and safety of Listeria monocytogenes-inoculated fresh-cut celery (Apium graveolens L.) during storage. *Postharvest Biology and Technology, 93*, 29–37. https://doi.org/10.1016/j.postharvbio.2014.02.005

González-Buesa, J., & Salvador, M. L. (2019). An Arduino-based low cost device for the measurement of the respiration rates of fruits and vegetables. *Computers and Electronics in Agriculture, 162*, 14–20. https://doi.org/10.1016/j.compag.2019.03.029

Hertog, M. L. A. T. M., Nicholson, S. E., & Whitmore, K. (2003). The effect of modified atmospheres on the rate of quality change in 'Hass' avocado. *Postharvest Biology and Technology, 29*, 41–53. https://doi.org/10.1016/S0925-5214(02)00211-9

Hertog, M. L. A. T. M., Peppelenbos, H. W., Evelo, R. G., & Tijskens, L. M. M. (1998). A dynamic and generic model of gas exchange of respiring produce: the effects of oxygen, carbon dioxide and temperature. *Postharvest Biology and Technology, 14*, 335–349. https://doi.org/10.1016/S0925-5214(98)00058-1

Ho, Q. T., Verboven, P., Verlinden, B. E., Schenk, A., Delele, M. A., Rolletschek, H., et al. (2010). Genotype effects on internal gas gradients in apple fruit. *Journal of Experimental Botany, 61*, 2745–2755. https://doi.org/10.1093/jxb/erq108

Jalali, A., Rux, G., Linke, M., Geyer, M., Pant, A., Saengerlaub, S., et al. (2019). Application of humidity absorbing trays to fresh produce packaging: Mathematical modeling and experimental validation. *Journal of Food Engineering, 244*, 115–125. https://doi.org/10.1016/j.jfoodeng.2018.09.006

Kader, A. A., Zagory, D., & Kerbel, E. L. (1989). Modified atmosphere packaging of fruits and vegetables. *Critical Reviews in Food Science and Nutrition, 28*, 1–30. https://doi.org/10.1080/10408398909527490

Kartal, S., Aday, M. S., & Caner, C. (2012). Use of microperforated films and oxygen scavengers to maintain storage stability of fresh strawberries. *Postharvest Biology and Technology, 71*, 32–40. https://doi.org/10.1016/j.postharvbio.2012.04.009

Kusuma, P., & Bugbee, B. (2020). An automated multi-chamber system for quantifying biological oxygen demand. Techniques and Instruments, Paper 16. Retrieved from https://digitalcommons.usu.edu/cpl_techniquesinstruments/16. Accessed June 15, 2021.

Kwon, M. J., Jo, Y. H., An, D. S., & Lee, D. S. (2013). Applicability of simplified simulation models for perforation-mediated modified atmosphere packaging of fresh produce. *Mathematical Problems in Engineering, Article ID.* , Article 267629. https://doi.org/10.1155/2013/267629

Lange, J., Büsing, B., Hertlein, J., & Hediger, S. (2000). Water vapour transport through large defects in flexible packaging: modeling, gravimetric measurement and magnetic resonance imaging. *Packaging Technology and Science, 13*, 139–147. https://doi.org/10.1002/1099-1522(200007)13:4<139::AID-PTS507>3.0.CO;2-E

Larsen, H., & Liland, K. H. (2013). Determination of O_2 and CO_2 transmission rate of whole packages and single perforations in microperforated packages for fruit and vegetables. *Journal of Food Engineering, 119*, 271–276. https://doi.org/10.1016/j.jfoodeng.2013.05.035

Lee, D. S. (2016). Carbon dioxide absorbers for food packaging applications. *Trends in Food Science & Technology, 57*, 146–155. https://doi.org/10.1016/j.tifs.2016.09.014

Lee, D. S., & Renault, P. (1998). Using pinholes as tools to attain optimum modified atmospheres in packages of fresh produce. *Packaging Technology and Science, 11*, 119–130. https://doi.org/10.1002/(SICI)1099-1522(199805/06)11:3<119::AID-PTS421>3.0.CO;2-N

Massman, W. J. (1998). A review of the molecular diffusivities of H_2O, CO_2, CH_4, CO, O_3, SO_2, NH_3, N_2O, NO, and NO_2 in air, O_2 and N_2 near STP. *Atmospheric Environment, 32*, 1111–1127. https://doi.org/10.1016/S1352-2310(97)00391-9

Mistriotis, A., Briassoulis, D., Giannoulis, A., & D'Aquino, S. (2016). Design of biodegradable bio-based equilibrium modified atmosphere packaging (EMAP) for fresh fruits and vegetables by using micro-perforated poly-lactic acid (PLA) films. *Postharvest Biology and Technology, 111*, 380–389. https://doi.org/10.1016/j.postharvbio.2015.09.022

Paul, D. R., & Clarke, R. (2002). Modeling of modified atmosphere packaging based on designs with a membrane and perforations. *Journal of Membrane Science, 208*, 269–283. https://doi.org/10.1016/S0376-7388(02)00303-4

Peelman, N., Ragaert, P., De Meulenaer, B., Adons, D., Peeters, R., Cardon, L., et al. (2013). Aplication of bioplastic for food packaging. *Trends in Food Science & Technology, 32*, 128–141. https://doi.org/10.1016/j.tifs.2013.06.003

Ratti, C., Rabie, H. R., & Raghavan, G. S. V. (1998). Modelling modified atmosphere storage of fres cauliflower using diffusion channels. *Journal of Agricultural Engineering Research, 69*, 343–350. https://doi.org/10.1006/jaer.1997.0254

Renault, P., Houal, L., Jacquemin, G., & Chambroy, Y. (1994). Gas exchange in modified atmosphere packaging. 2: Experimental results with strawberries. *International Journal of Food Science and Technology, 29*, 379–394. https://doi.org/10.1111/j.1365-2621.1994.tb02080.x

Renault, P., Souty, M., & Chambroy, Y. (1994). Gas exchange in modified atmosphere packaging. 1: A new theoretical approach for micro-perforated packs. *International Journal of Food Science and Technology, 29*, 365–378. https://doi.org/10.1111/j.1365-2621.1994.tb02079.x

Rennie, T. J., & Tavoularis, S. (2009a). Perforation-mediated modified atmosphere packaging. Part I. Development of a mathematical model. *Postharvest Biology and Technology, 51*, 1–9. https://doi.org/10.1016/j.postharvbio.2008.06.007

Rennie, T. J., & Tavoularis, S. (2009b). Perforation-mediated modified atmosphere packaging. Part II. Implementation and numerical solution of a mathematical model. *Postharvest Biology and Technology, 51*, 10–20. https://doi.org/10.1016/j.postharvbio.2008.06.012

Saltveit, M. E. (2012). *Measuring respiration. Postharvest biology and technology (PLS 172) lecture handout* (p. 2021). Davis, California: University of California, (Accessed June) http://ucce.ucdavis.edu/files/datastore/234-20.pdf.

Sousa-Gallagher, M. J., & Mahajan, P. V. (2013). Integrative mathematical modelling for MAP design of fresh-produce: Theoretical analysis and experimental validation. *Food Control, 29*, 444–450. https://doi.org/10.1016/j.foodcont.2012.05.072

Sousa-Gallagher, M. J., Mahajan, P. V., & Mezdad, T. (2013). Engineering packaging design accounting for transpiration rate: Model development and validation with strawberries. *Journal of Food Engineering, 119*, 370–376. https://doi.org/10.1016/j.jfoodeng.2013.05.041

Techavises, N., & Hikida, Y. (2008). Development of a mathematical model for simulating gas and water vapor exchanges in modified atmosphere packaging with macroscopic perforations. *Journal of Food Engineering, 85*, 94–104. https://doi.org/10.1016/j.jfoodeng.2007.07.014

Varriano-Marston, E., 2006, Registered microperforated films for modified/controlled atmosphere packaging. US Patent 7083837B1.

Waghmare, R. B., Mahajan, P. V., & Annapure, U. S. (2013). Modelling the effect of time and temperature on respiration rate of selected fresh-cut produce. *Postharvest Biology and Technology, 80*, 25–30. https://doi.org/10.1016/j.postharvbio.2013.01.012

Winotapun, C., Aontee, A., Inyai, J., Pinsuwan, B., & Daud, W. (2021). Laser perforation of polyethylene terephthalate/polyethylene laminated film for fresh produce packaging application. *Food Packaging and Shelf Life, 28*, Article 100677. https://doi.org/10.1016/j.fpsl.2021.100677

Winotapun, C., Kerddonfag, N., Daud, W., Chinsirikul, W., Takarada, W., & Kikutani, T. (2018). Effect of biaxial-simultaneous stretching conditions on OTR and CO_2 permeation of CO_2 laser perforated poly(lactic acid) film. *Packaging Technology and Science, 31*, 545–556. https://doi.org/10.1002/pts.2381

Xanthopoulos, G., Koronaki, E. D., & Boudouvis, A. G. (2012). Mass transport analysis in perforation-mediated modified atmosphere packaging of strawberries. *Journal of Food Engineering, 111*, 326–335. https://doi.org/10.1016/j.jfoodeng.2012.02.016

Zhang, J., 2015, A mathematical model for predicting optimal micro-perforated packaging, master thesis, Michigan State University, East Lansing, Michigan, ProQuest 1605005. Retrieved from https://d.lib.msu.edu/etd/3591/datastream/OBJ/View/. Accessed June 15, 2021.

Zhang, Y., Liu, Q., & Geng, X. (2017). Modelling of modified atmosphere packaging based on conventional polymeric films and perforated films. In S. Pareek (Ed.), *Novel Postharvest Treatments of Fresh Produce* (pp. 533–556).